Two Phase Bubble Columns: the Determinants of the Flow Regime Transitions

Two Phase Bubble Columns: the Determinants of the Flow Regime Transitions

N Varallo[1*], G Besagni[1], R Mereu[1] and F Inzoli[1]

[1] Politecnico di Milano, Department of Energy, Via Lambruschini 4, Milan 20156, Italy

* Corresponding author: nicolo.varallo@polimi.it

Abstract. The fluid dynamics in large-diameter bubble columns can be described by an analytical relation between two global flow parameters, the drift flux and the gas holdup. This relation, named bubble column operating curve, builds on five flow regime transitions. In order to determine the variables influencing the flow regime transitions, a statistical approach was derived by coupling: (1) the ordinary least squares method (OLS) to determine the relationship between the variables, (2) the variance inflation factor (VIF) to check for multicollinearity issues, and (3) the least absolute shrinkage and selection operator (LASSO), to select suitable variables. It was found that the geometrical characteristics of the sparger strongly influence the flow regime transitions, and uniform aeration is essential for all the regimes to exist. Increasing the superficial liquid velocity in the counter-current mode destabilises the mono-dispersed and poly-dispersed homogeneous flow regimes. As for the aspect ratio, an increase in the column aspect ratio slightly destabilises the existing flow regimes. The statistical method identifies viscosity as the only significative variable concerning the liquid phase properties.

1. Introduction

Bubble columns are gas-liquid reactors widely used in many industrial applications. They are of considerable interest in chemical processes involving reactions like oxidation, chlorination, alkylation, polymerization, and hydrogenation, as well as in the production of synthetic fuels and biochemical processes such as fermentation and biological wastewater treatment. Bubble columns offer several advantages, such as excellent heat and mass transfer between the phases, high durability, and low operating and maintenance costs due to the absence of moving parts [1].

In its simplest configuration, a bubble column consists of a vertical vessel without internals where a gas distributor disperses the gas phase into bubbles or coalescence-induced structures entering the column. The liquid flow rate can be fed co-currently or counter-currently to the rising bubbles, or it may be zero (batch operating mode). Despite the simple column layout, bubble column hydrodynamics is very complex due to the interactions between the continuous and the dispersed phases. The coupling between the phases physically manifests in the flow regimes.

Besagni (2021) [2] proposed a novel physical-based theory for the description of the fluid dynamics in large-diameter bubble columns (bubble column diameter greater than 0.15m at ambient operating conditions). The theory states that the fluid dynamics in large-diameter systems can be described by an analytical relation (bubble column operating curve) between two global flow parameters: the drift flux and the gas holdup. The drift flux, J, is defined as the volumetric flux of either component relative to a surface moving at volumetric average velocity expressed as follows.

$$J = U_G(1 - \varepsilon_G) \pm U_L\varepsilon_G \quad (1)$$

In Equation (1), ε_G is the global gas holdup, U_G is the superficial gas velocity, and U_L is the superficial liquid velocity. The sign on the right-hand side of Equation (1) depends on the bubble column operating mode: co-current mode (+) or counter-current mode (-); in the batch mode $U_L = 0$.

The bubble column operating curve (Figure 1) builds on five flow regime transitions. Consequently, six flow regimes can be encountered in large-diameter bubble columns. The six flow regimes emerging upon an increase in the gas flow rate at fixed system design parameters, operating mode, and phases properties are: (1) mono-dispersed homogeneous flow regime, (2) poly-dispersed homogeneous flow regime, (3) transition flow regime without coalescence-induced structures, (4) transition flow regime with coalescence-induced structures, (5) pseudo-heterogeneous flow regime, and (6) pure-heterogeneous flow regime (Figure 1).

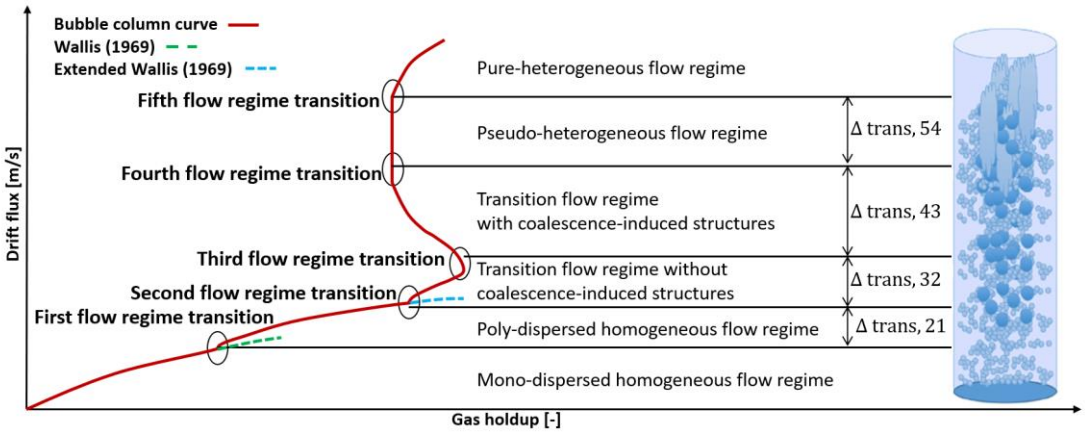

Figure 1. Flow regime and flow regime transitions in a large diameter bubble column [2]. The symbol Δ indicates the difference in drift flux and gas holdup between a flow regime transition and the previous one.

Changing the system design and/or the phase properties and/or the operating mode induces a change in the boundaries between the flow regimes without influencing the flow regime properties themselves [2]. Consequently, the bubble column fluid dynamics can be described and predicted a-priori via correctly modelling the flow regime transitions.

This paper is organised as follows. Section 2 describes the variables used to conduct the statistical analysis. Section 3 presents the statistical approach. The results obtained are presented and discussed in Section 4. Finally, conclusions are drawn, and future studies are proposed.

2. Dependent Variables and Predictors

As for the dependent variables, the flow regime theory [2] was applied to determine the flow regime transitions coordinates ($\varepsilon_{G,\text{trans}}$ and $U_{G,\text{trans}}$) of different large-diameter bubble columns operating in batch and counter-current mode with different gas distributors, aspect ratio values, and liquid phase properties (Table 1).

From a practical perspective the flow regimes transitions can be identified as follows.

- **First flow regime transition.** The transition can be detected by comparing the experimental drift flux values (J_E) with the theoretical drift flux curve (J_T) proposed by Wallis (1969) [3], written in terms of bubble swarm velocity (v_b):

$$J_T = v_b(1 - \varepsilon_G) \quad (2)$$

The evaluation of the bubble swarm velocity is a matter of discussion; in this study, the approach proposed by Krishna et al. (1999) [4] is considered:

$$v_b = U_t(1 - \varepsilon_G)^n \tag{3}$$

Where n is a fluid-dependent variable ($n \approx 2$ for water-based solutions) and U_t is the terminal velocity of an isolated bubble obtained fitting the experimental data. In the mono-dispersed homogeneous flow regime J_E equals J_T and the transition to the poly-dispersed homogeneous flow regime occurs when:

$$J_E \neq J_T \tag{4}$$

- **Second flow regime transition**. The flow regime theory states that the poly-dispersed homogeneous flow regime builds upon the mono-dispersed one. Consequently, the approach previously described can be applied to determine the second flow regime transition after a correct change in the variables (the first flow regime transition must be considered as the new origin):

$$\varepsilon'_G = \varepsilon_G - \varepsilon_{G,\text{trans},1} \tag{5}$$

$$U'_G = U_G - U_{G,\text{trans},1} \tag{6}$$

Therefore, the bubble column drift flux referred to the new coordinates is:

$$J'_E = U'_G(1 - \varepsilon'_G) \pm U_L\varepsilon'_G \tag{7}$$

Considering a new theoretical drift flux curve (J'_T), the transition point can be detected when:

$$J'_E \neq J'_T \tag{8}$$

- **Third flow regime transition.** The third flow regime transition coincides with the maximum J_E with respect to ε_G:

$$\varepsilon_{G,\text{trans},3} = \max\left(\varepsilon_G(J_E)\right) \tag{9}$$

- **Fourth flow regime transition**. When the transition flow regime with coalescence-induced structures is established, an increase in the gas flow rate (in terms of drift flux) is followed by a decrease in the gas holdup. On the contrary, the pseudo heterogeneous flow regime is characterized by a constant value of gas holdup with respect to an increase in the gas flow rate. Consequently, the fourth flow regime transition can be determined based on the constant value of ε_G at high drift flux values:

$$\frac{\partial\varepsilon_G(J_E)}{\partial J_E} = 0 \tag{10}$$

- **Fifth flow regime transition**. The fifth flow regime transition is observed when the gas holdup begins to increase again due to an increment in the drift flux:

$$\varepsilon_G(J_E) \neq \varepsilon_{G,\text{trans},4} \tag{11}$$

Given the flow regime transitions coordinates, only the first flow regime transition was considered in "*absolute terms*" (i.e. $\varepsilon_{G,\text{trans},1}$ and $U_{G,\text{trans},1}$) since the others and the corresponding dependent variables were defined relative to the previous transition (i.e. $\Delta\varepsilon_{G,\text{trans},ij} = \varepsilon_{G,\text{trans},i} - \varepsilon_{G,\text{trans},j}$ and $\Delta U_{G,\text{trans,ij}} = U_{G,\text{trans},i} - U_{G,\text{trans},j}$, with $j = i - 1$ and $i = 2 \dots 5$). In this way, if a flow regime does not exist, $\Delta\varepsilon_{G,\text{trans}}$ and $\Delta U_{G,\text{trans}}$ equal zero; they are different from zero otherwise. $\Delta\varepsilon_{G,\text{trans},54}$ is useless to describe the transition to the pure heterogeneous flow regime [2] and so only $\Delta U_{G,\text{trans},54}$ was considered.

Concerning the predictors (i.e., independent variables), they were divided into three different macro-categories: (1) geometrical characteristics of the column, (2) operating conditions, and (3) liquid phase properties (Table 2).

Table 1. Bubble column configurations analysed.

Ref.	Liquid phase	D_H [m]	AR [-]	Sparger	d_0 [mm]	Operating conditions
[6]	Water	0.2	1	Perforated plate	1	Open tube; batch
[7]	Water	0.158	0.105	Perforated plate	2	Open tube; batch
[8]	Water	0.156	0.125	Perforated plate	0.5	Open tube; batch
[9]	Water	0.29 – 0.4	0.34 → 4.14	Perforated plate	0.5	Open tube; batch
[10]	Water	0.15 – 0.4	10.67	Perforated plate	0.5	Open tube; batch
[11]	Water	0.29	0.176	Perforated plate	0.5	Open tube; batch
[12]	Water	0.15 – 0.38	2.857	Perforated plate	0.5	Open tube; batch
[13]	$CaCl_2$ solution	0.15	2.857	Perforated plate	0.5	Open tube; batch
[2]	Water	0.24	1 → 15	Perforated plate	0.5 - 1	Open tube; batch
[2]	Water	0.24	1 → 15	Needle	0.5	Open tube; batch
[2]	Water	0.24	1 → 15	Spider	2 → 4	Open tube; batch
[2]	Water	0.24	12.5	Pipe	3	Open tube – annular gap; Batch – counter-current
[2]	NaCl solution	0.24	5 → 10	Spider	2 → 4	Open tube; batch
[2]	EtOH solution	0.24	5 → 12.5	Spider	2 → 4	Open tube; batch
[2]	MEG solution	0.23	5 → 12.5	Spider	2 → 4	Open tube; batch

Table 2. Independent variables.

Column geometrical characteristics	Operating conditions	Liquid phase properties
Column diameter (D_H)	Superficial liquid velocity (U_L)	Viscosity (μ)
Sparger type	Presence of internals	Density (ρ)
Sparger hole diameter (d_0)		Surface tension (σ)
Free area[a] (A_f)		
Aspect ratio (AR)		

[a] The free area is the ratio between the total area of the sparger openings and the cross-sectional area of the column.

3. Statistical Methods

Following the approach proposed by Varallo et al. (2023) [14], the statistical method consists of OLS to determine the relations between dependent and independent variables, VIF to check for multicollinearity issues, and LASSO to select the significative predictors in describing the flow regime transitions. Subsequently, a segmentation of bubble columns with similar flow regime transitions coordinates is proposed, by using a CART approach.

The statistical approach consists of five steps (Figure 2a). In the first step, a dependent variable is selected out of $\varepsilon_{\text{trans},1}$, $U_{G,\text{trans},1}$, $\Delta\varepsilon_{G,\text{trans,ij}}$ and $\Delta U_{G,\text{trans,ij}}$. In the second step, a class of predictors is selected out of the three groups listed in Section 2. In the third step, the regression procedure is applied to the selected dependent variable and the selected class of predictors ("*partial regression*

models"). Subsequently, the above-described steps (#1 to #3) are iterated until all the dependent variables have been considered and all the "*partial regression models"* have been obtained. In the fourth step the predictors found significant after the regression procedure are coupled, and the regression analysis is performed again to obtain the "*aggregate regression models*". Steps 2-3 are iterated until all the classes of predictors have been evaluated with respect to the dependent variables and all the "*aggregate regression models*" have been obtained. The OLS-VIF-LASSO procedure applied at step#3 and step#4 is shown in Figure 2b.

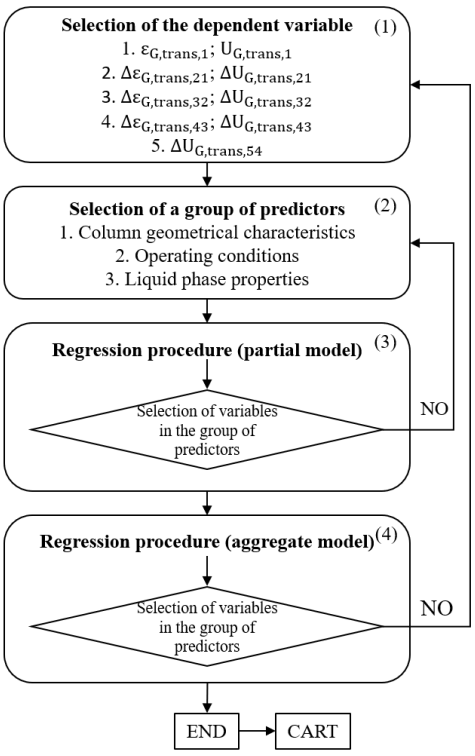

Figure 2a. Procedure overview.

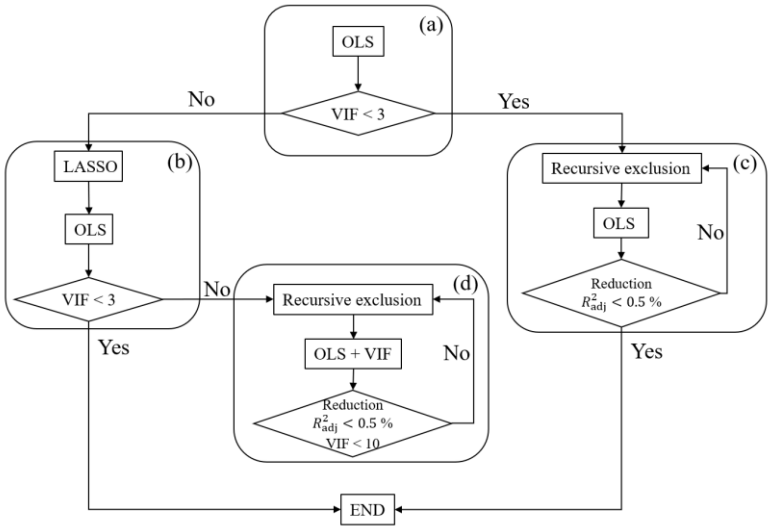

Figure 2b. OLS-VIF-LASSO procedure overview.

4. Results and Discussion

Table 3 and Table 4 display the adjust coefficient of determination (R^2_{adj}) for the partial and aggregate regression models. The geometrical characteristics of the column mainly influence the flow regime transitions, expect the second flow regime transition, where the influence of the operating conditions is more significant than the column geometrical characteristics. The liquid phase properties primarily influence $U_{G,\text{trans},1}$ ($R^2_{\text{adj}} = 14.28\,\%$) rather than $\varepsilon_{G,\text{trans},1}$ ($R^2_{\text{adj}} = 2.94\,\%$). In contrast, it does not explain the variance of the second transition ($R^2_{\text{adj}} = 0.62\,\%$ and $R^2_{\text{adj}} = 0.63\,\%$ for $\Delta\varepsilon_{G,\text{trans},21}$ and $\Delta U_{G,\text{trans},21}$, respectively). The partial regression models referred to the operating conditions and liquid phase properties for the third, fourth and fifth flow regime transitions show a negative or zero value of R^2_{adj}. The reason is that these transitions are present only when the column operates with the perforated plate and needle spargers, which provide uniform aeration. In the experimental data analysed to create the dataset, the perforated plate sparger was tested only in batch mode with water as the liquid phase (Table 1). Therefore, the influence of the operating conditions and liquid phase properties on the third and fourth flow regime transitions cannot be analysed.

Table 3. Coefficient of determinations: gas holdup.

R^2_{adj}	$\varepsilon_{G,\text{trans},1}$	$\Delta\varepsilon_{G,\text{trans},21}$	$\Delta\varepsilon_{G,\text{trans},32}$	$\Delta\varepsilon_{G,\text{trans},43}$
Geometrical characteristics	56.75 %	29.64 %	34.49 %	52.41 %
Operating conditions	8.34 %	22.50 %	-0.06 %	0.00 %
Liquid phase properties	2.94 %	0.62 %	-3.00 %	-2.72 %
Aggregated models	60.63 %	34.87 %	34.49 %	52.41 %

Table 4. Coefficient of determinations: superficial gas velocity.

R^2_{adj}	$U_{G,\text{trans},1}$	$\Delta U_{G,\text{trans},21}$	$\Delta U_{G,\text{trans},32}$	$\Delta U_{G,\text{trans},43}$	$\Delta U_{G,\text{trans},54}$
Column geometrical characteristics	54.99 %	17.20 %	39.94 %	51.06 %	58.70 %
Operating conditions	26.68 %	40.13 %	-0.57 %	0.00 %	1.20 %
Liquid phase properties	14.28 %	0.63 %	-2.60 %	-2.67 %	-0.83 %
Aggregated models	64.65 %	43.41 %	39.94 %	51.06 %	58.70 %

The regression model results (Table 5 and Table 6 present an example) indicate that $\varepsilon_{G,\text{trans},1}$ and $U_{G,\text{trans},1}$ decrease as the distributor's holes diameter and aspect ratio increase, leading to a destabilization of the mono-dispersed homogeneous flow regime. A counter-current motion of the liquid causes the same effect, decreasing $U_{G,\text{trans},1}$ concerning the batch mode.

Regarding the second flow regime transition, the variables of interest are the sparger holes diameter, the aspect ratio, the superficial liquid velocity, and the free area. An increase in the sparger holes diameter decreases $\Delta\varepsilon_{G,\text{trans},21}$ and increases $\Delta U_{G,\text{trans},21}$. The column aspect ratio influences only $\Delta\varepsilon_{G,\text{trans},21}$, and an increase in its value lead to a decrease in $\Delta\varepsilon_{G,\text{trans},21}$. An increase in the free area causes a reduction in $\Delta U_{G,\text{trans},21}$, but it does not influence $\Delta\varepsilon_{G,\text{trans},21}$. Finally, the poly-dispersed homogeneous flow regime is destabilized by an increase in the superficial liquid velocity in the counter-current mode.

Regarding the other flow regime transitions, the only variables of interest are the geometrical characteristics of the column. In particular, a dominant role is played by the type of gas distributor. The uniform aeration provided by the needle and perforate plate spargers is necessary to ensure that the third, fourth, and fifth flow regime transitions exist.

The graphical representation of the results, provided by the regression trees (Figure 3 and Figure 4 show an example), can be immediately used to identify the boundaries between the flow regimes.

Table 5. Output of the regression procedure: aggregate regression model for $\Delta\varepsilon_{G,\text{trans},21}$.

	Coefficient	**Standard error**	**t-value**	**Pr (> t)**	**VIF**
Intercepts	0.123	0.012	10.015	<2E-16	-
Sparger holes diameter	-0.008	0.006	-1.376	0.171	2
Aspect ratio	-0.005	0.001	-3.615	4.4E-04	1.82
Superficial liquid velocity	0.751	0.228	3.287	0.001	1.33

Table 6. Output of the regression procedure: aggregate regression model for $\Delta U_{G,\text{trans},21}$.

	Coefficient	**Standard error**	**t-value**	**Pr (> t)**	**VIF**
Intercepts	0.220	1.12E-01	1.973	0.051	-
Sparger hole diameter	0.002	1.48E-03	1.274	0.205	1.67
Free area	0.02	0.550	2.146	0.038	1.82
Superficial liquid velocity	0.469	0.006	7.606	7E-12	1.34

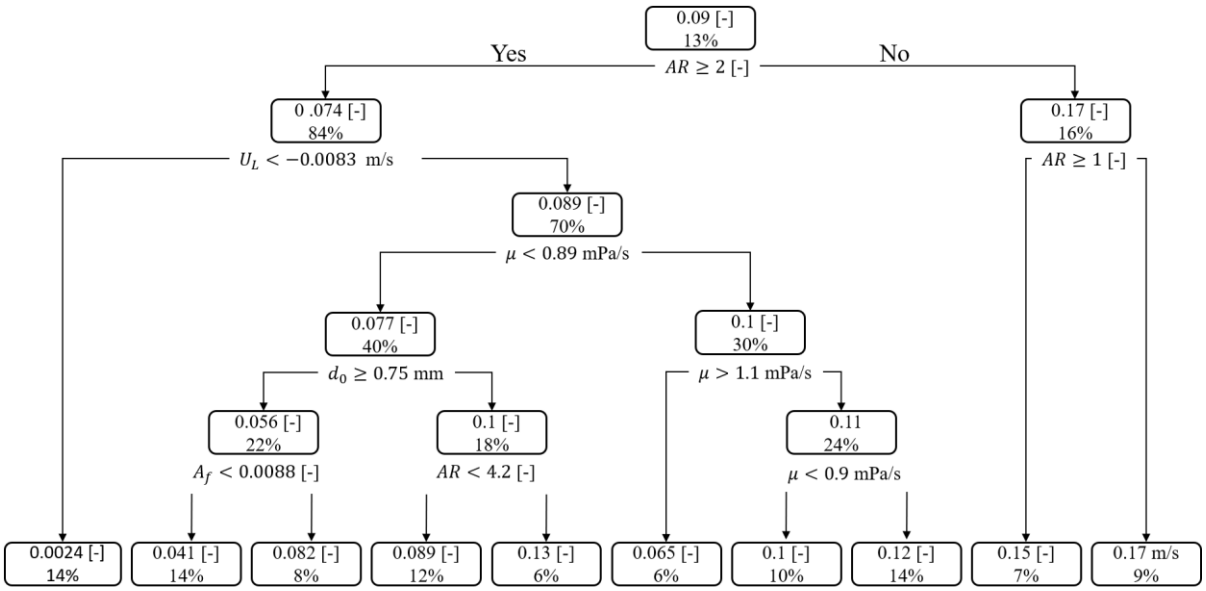

Figure 3. Regression tree: $\Delta\varepsilon_{G,\mathrm{trans},21}$

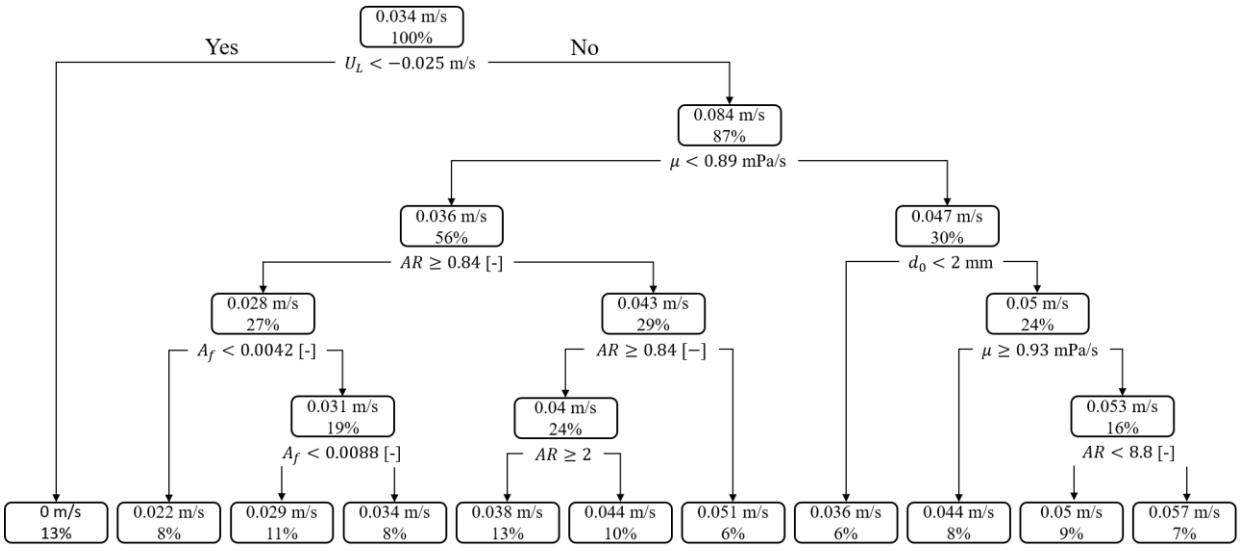

Figure 4. Regression tree: $\Delta U_{G,\mathrm{trans},21}$

5. Conclusions

The statistical method defined in this study has proven to be an interesting and powerful tool for describing bubble columns fluid dynamics. The graphical representation of the results, provided by the regression trees, can be immediately used to identify the boundary between the flow regimes and their fluid dynamics properties. Once the design characteristics of the column and the working fluids are defined, the regime transitions can be identified, and an approximate bubble column characteristic curve can be drawn (Figure 5).

Future studies should extend the applicability of the approach proposed by expanding the dataset considered in this study. In particular, the dataset should be expanded as follows.

- Perforated plate and needle spargers should be considered with liquid phases different from water to include the effects of the liquid properties on the third, fourth and fifth flow regime transitions.
- Columns operating in co-current mode should be added for better understanding the influence of the surface liquid velocity on flow regime transitions.
- Columns operating at different temperatures and pressures should be considered since they are of interest for industrial applications.

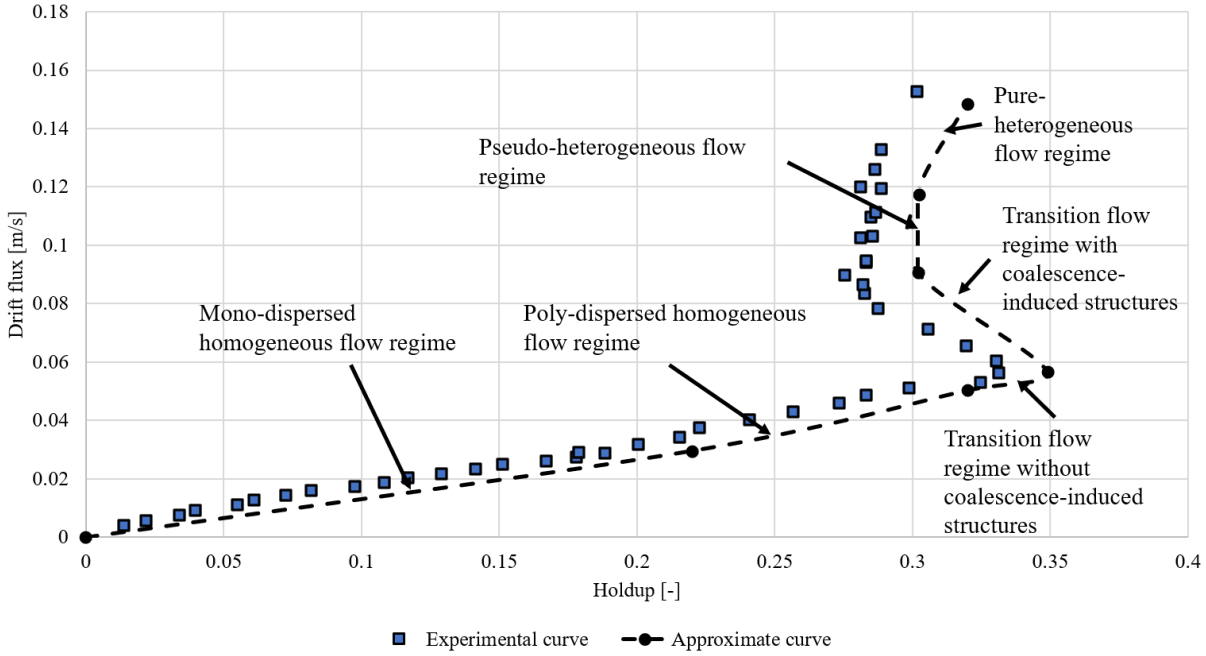

Figure 5. Example of statistically derived bubble column characteristics curve.

6. References

[1] Shaikh A and Al-Dahhan M H 2007 Int. J. *Chem. React. Eng.* **5**(1)
[2] Besagni G *Int. J. Multiph. Flow* **135** 103510
[3] Wallis G.B 1969 One-Dimensional Two-Phase Flow (New York: McGraw-Hill)
[4] Krishna R, Ellenberger J and Maretto C 1999 Int. Commun. Heat Mass 26 467-75
[5] Krishna R, Urseanu M I and Dreher A J 2000 *Chem. Eng. Process* **39**(4) pp 371–378
[6] Deckwer W D, Burckhart R and Zoll G 1974 *Chem. Eng. Sci.* **29**(11) pp 2177–2188
[7] Wilkinson P M, Spek A P and van Dierendonck L L 1992 *AIChE* **38**(4) pp 544–554
[8] Letzel H M, Schouten J C, Krishna R and Van Den Bleek C M 1997 *Chem. Eng. Sci.* **52**(24) pp 4447–4459
[9] Ruzicka M, Drahoš J and Thomas N H 2001 *Chem. Eng. Sci.* **56**(21-22) pp 6117–6124
[10] Vandu C O, Koop K and Krishna R 2004 *Chem. Eng. Technol.* **27**(11) pp 1195–1199
[11] Chilekar V P, Singh C, Van Der Schaaf J, Kuster B F M and Schouten J 2007 *AIChE* **53**(7) pp 1687–1702
[12] Ruzicka M C, Vecer M M, Orvalho S and Drahos J 2008 *Chem. Eng. Sci.* **63**(4) pp 951–967
[13] Yang N, Chen J, Ge W and Li J 2010 *Chem. Eng. Sci.* **65**(1) pp 517–526
[14] Varallo N, Besagni G and Mereu R 2023 *Chem. Eng. Trans.* **100**, 361-366.
[15] Besagni G and Borgarello M 2018 *Energy* **165** pp 369–386